STATISTICAL STUDIES OF ONE-DIMENSIONAL SPATIOTEMPORAL CHAOS IN THE PRINTER'S INSTABILITY

CUIJUN LU

Statistical Studies of One-Dimensional Spatiotemporal Chaos in the Printer's Instability

by

Cuijun Lu, B.Sc. (Hons.)

A THESIS SUBMITTED TO THE SCHOOL
OF GRADUATE STUDIES IN PARTIAL FULFILLMENT
OF THE REQUIREMENTS FOR THE DEGREE OF
MASTER OF SCIENCE

DEPARTMENT OF PHYSICS AND PHYSICAL OCEANOGRAPHY
MEMORIAL UNIVERSITY OF NEWFOUNDLAND

APRIL 1996

ST. JOHN'S NEWFOUNDLAND

ISBN 0-612-17614-2

Canada

Abstract

A number of statistical techniques are used to study spatiotemporal chaos in a one dimensional pattern of fingers which form at a driven oil air meniscus. It is shown that the long time average of the chaotic pattern is structureless. The rms deviation between finite and infinite time averages decreases approximately as a power law in the averaging time. The results suggest that for short averaging times (i.e., less than about 50 s) the short time average approaches the long time average much like a Gaussian variable, but that for longer averaging times the approach to the infinite-time average is significantly slower than that of a simple Gaussian process. Generally, the early time behavior of the cross-correlation coefficient between patterns recorded at different times decays exponentially around the threshold of STC. The spatial autocorrelation function of the chaotic pattern has a decaying oscillatory tail that is approximately the product of a cosine and a decaying exponential. The correlation length is about equal to the wavelength of the basic pattern.

Acknowledgements

It is a great pleasure to thank my supervisor, Dr. J. R. de Bruyn, for encouraging me and providing me with the opportunity to work on an exciting experiment in spatiotemporal chaos. I am grateful for his invaluable assistance and excellent guidance at all stages of this work. His constructive suggestions and comments made a great contribution to the completion of this thesis. I also acknowledge the generous support from Dr. de Bruyn's NSERC grant, the Graduate Fellowship from Memorial University of Newfoundland and Teaching Assistantship from the Department of Physics and Physical Oceanography during my graduate studies. Finally, I would like to express my everlasting gratitude to my parents who have always encouraged me to do my best. This thesis is dedicated to them.

Table of Contents

List of Figures

Chapter 1

Introduction

1.1 Spatiotemporal Chaos

Patterns which form in hydrodynamical systems driven out of equilibrium have recently been the subject of much interest [1]. Close to equilibrium, the system is spatially uniform. As it is driven further from equilibrium by changing an appropriate control parameter, the system undergoes a transition to a state with an organized flow pattern. As the control parameter is further increased, the pattern becomes less organized. When a pattern varies irregularly in both space and time, it is called spatiotemporal chaos (STC). Fig. 1.1 shows an example of spatiotemporal chaos in the system studied in this thesis. The figure shows a sequence of video lines, taken through a one-dimensional pattern of fingers which form at a driven oil air interface, and illustrates that the fingers move irregularly along the interface. This thesis describes work aimed at characterizing the dynamics of this spatiotemporal chaotic pattern using straightforward statistical methods.

The characterization of STC is a challenge in nonlinear physics. Suitable generally applicable methods for the analysis of such complex patterns have been sought for a long time. In the last two decades, significant progress has been achieved in

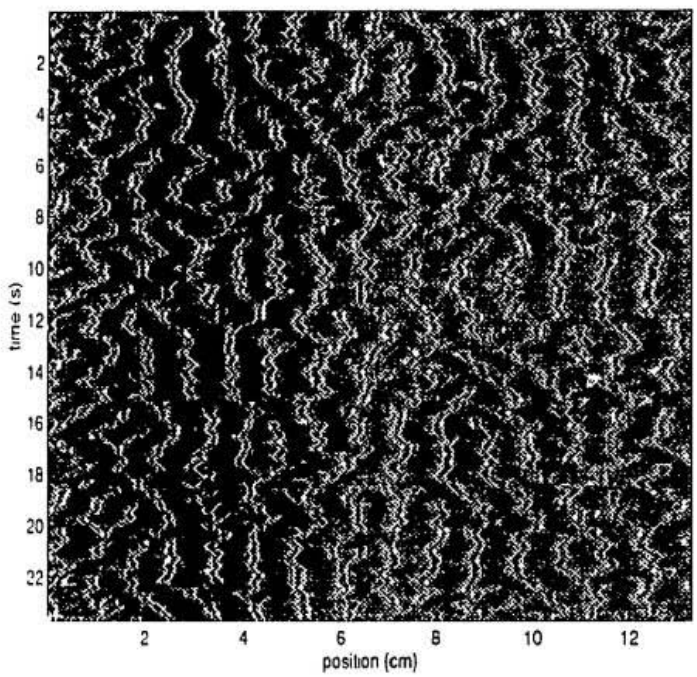

Figure 1.1: This spatiotemporal image with background subtracted shows the STC of the printer's instability. The thesis describes work aimed at characterizing the dynamics of the STC using straightforward statistical methods.

the experimental analysis of instabilities and hydrodynamical flows using techniques such as laser velocimetry and image processing, and computerized data processing and experiment control. The experimental work has benefited from the close linkage with new theoretical work based on instability and bifurcation theory. On the other hand, the theoretical study of the succession of instabilities obtained by increasing the control parameter requires nonlinear analysis which extends far beyond the classical studies in the field. Hence a few relatively simple systems, such as Rayleigh-Bénard convection and Taylor-Couette flow, have become very popular as prototypes of complex behavior where nonlinear theories of pattern formation may easily be tested.

Unfortunately, the invariant quantities used to characterize model nonlinear dynamical systems (attractor dimension, Kolmogorov – Sinai entropy, etc.) have not been found generally useful for the analysis of experimental data. This indicates that a deterministic description of STC is hard to establish in practice, though in principle it could be possible. On the other hand, statistical methods have been productively employed to describe STC in some experiments ([2] [5]). As there are so many degrees of freedom involved in the dynamics of a spatiotemporally chaotic pattern, relatively standard statistical approaches may be the only practical route to both experimental characterization and meaningful comparisons between experiment and theory.

One of the simplest statistical measures is the time average of instantaneous

fluctuating patterns. Experimentally, this can be obtained by taking video images of the patterns and averaging the images over time. It has been used earlier in the study of dynamical systems ([6] [8]). In some recent experiments, the time-average of a spatiotemporally chaotic pattern has been shown to have nontrivial spatial structure. For example, Gluckman *et al.* [9] studied STC in the Faraday surface wave instability using various statistical methods, including the time average. They observed highly ordered time averaged patterns due to a high degree of phase coherence of the chaotic instantaneous patterns. They explained their time-averaged patterns as arising from amplitude and phase fluctuations about a base wave pattern. Their results will be discussed further in section 1.2.

Another statistical quantity is the pattern's correlation length ξ. This length can become very short in STC as many degrees of freedom are involved in the dynamics [1]. The correlation length was used by Hohenberg and Shraiman [10] as one of three characteristic length scales of a spatiotemporally chaotic system, the other two being the dissipation scale l_D, which is the characteristic length at which energy is dissipated, and the excitation scale l_E, the length scale at which energy is injected into the system. The correlation length is defined through a correlation function

$$C'(r) = \langle \delta U'(r,t)\delta U'(0,t)\rangle \tag{1.1}$$

where $\delta U'(r,t)$ represents the fluctuations of the dynamical variable $U(r,t)$ from its time average value at position r and $\langle\ \ \rangle$ denotes a long time average. Translational

invariance is assumed, which means the results should not depend on the choice of origin. $C'(r)$ is expected to decay as

$$C'(r) \approx exp(-r/\xi) \tag{1.2}$$

where ξ is the correlation length. The correlation length is the length scale over which a spatially coherent pattern can exist. A finite correlation length implies that quantities measured inside a correlation volume will have nontrivial statistics. For small systems, such that $\xi > L$, where L is the size of the system, fluctuations in the dynamical variables may be chaotic in time but are constrained to be coherent in space. Spatiotemporal chaos, on the other hand, occurs when $\xi << L$, so that fluctuations are incoherent in space as well as in time. STC is characterized by the chaotic evolution of coherent structures roughly the size of the correlation length ξ.

In thermal convection, statistical properties of the total transport (e.g. averages or power spectra) provide a meaningful way to characterize STC [1]. In Rayleigh Bénard convection [11] and parametrically forced surface waves [4], spatial auto correlation functions have been used to characterize STC. The decay of temporal correlation function can also be used to study the pattern dynamics and the onset of STC.

In the rest of this chapter, we focus on previous work on STC in thermal convection and hydrodynamic surface and interface waves. Several experimental and theoretical examples of spatiotemporal chaos are briefly reviewed in section 1.2.

1.2 Previous experimental work on STC

A variety of fluid dynamical experiments in the past few years have revealed states that are apparently spatiotemporally chaotic, although a complete characterization of the pattern dynamics is difficult to achieve. Experimentally, STC has been studied in, for example, Rayleigh-Bénard convection [12], the Faraday instability [1][13], the Taylor-Couette system [14], the Taylor-Dean system [15][16], roll coating experiments including the printer's instability [17], *etc*. Theoretically, the one dimensional Swift-Hohenberg model of convection [18] and the Kuramoto-Sivashinshy (KS) equation [18] have shown STC which can be reached by a transition in which the system passes through a spatiotemporally intermittent state. The complex Ginzburg-Landau equation also shows spatiotemporal chaos in both one and two dimensions. In 1D, Shraiman *et al.* [19] implemented a numerical study of the Ginzburg-Landau equation in a large system and identified two different chaotic states, one with "space-time defects" and one with only phase fluctuations and no defects. In a 2D model, for example, a STC in plasma has been discussed by Newell *et al.* [20], focusing on the function of coherent structures in turbulent transport and dissipation.

Rayleigh-Bénard convection has been studied extensively, both experimentally [21][22], and theoretically [21][23]. Rayleigh-Bénard convection in layers of large horizontal extent has proven to be a useful system for the study of STC in pattern

forming systems. The experimental set-up for studying Rayleigh-Bénard convection consists of two horizontal rigid plates with a thin fluid layer confined between them. When the bottom plate is heated, a temperature difference ΔT between the top and bottom of the layer is produced. For small temperature gradients, the fluid remains in a conductive state but, on increasing the temperature difference between the horizontal fluid boundaries, the gradient may reach a threshold where this conductive state becomes unstable. Beyond this threshold (instability or bifurcation point), convection sets in as cellular structures associated with periodic spatial variations of the hydrodynamic fluid velocity field and of the temperature field. Several types of structures may be obtained according to the experimental conditions: rolls, hexagons, squares, traveling or standing waves. On increasing the bifurcation parameter further, these patterns may in turn become unstable, causing successive bifurcations to occur and driving the system to chaos. Such chaos appears to involve the repetitive nucleation and elimination of defects in the pattern of rolls ([24]-[26]). Several types of defects have been observed, including disclinations, dislocations, and grain boundaries.

Spatial autocorrelation functions have been used to characterize STC in Rayleigh Bénard convection. Morris *et al.* [11] studied chaotic convection patterns in a cylindrical cell with a large aspect ratio. Using a structure function $S(\mathbf{k})$, they define an average wave vector $\langle k \rangle$ and a correlation length $\xi = [\langle k^2 \rangle - \langle k \rangle^2]^{-1/2}$. $S(\mathbf{k})$ is the

time average of the square of the modulus of the spatial Fourier transform of a shadowgraph of the convection rolls and provides quantitative information regarding the spatial scales of the roll patches. They found that ξ decreases with an increase in the reduced temperature difference ϵ ($\epsilon \equiv \Delta T/\Delta T_c - 1$) and could be fitted by a power law of the form $\xi = \xi_0 \epsilon^{-\nu}$, where $\xi_0 = (2.1 \pm 0.1)d$ (d is the height of the experimental cell) and $\nu = 0.13 \pm 0.05$. Daviaud *et al.* [27] computed spatial correlation functions of the intensity of convective patterns in a rectangular geometry. They define the correlation length ξ through the correlation function and measured ξ for different values of ϵ. They found the envelope of the correlation function to have an exponential decay with increasing ϵ. They showed the dependence of ξ on ϵ and noted a change of behavior near $\epsilon = 370$, the threshold of spatiotemporal intermittency (STI), where a sudden decrease of ξ was observed. STI is characterized by the dynamical coexistence in time and space of chaotic and laminar domains. Below the threshold of STI, the correlation length is on the order of the length of the system: $\xi \simeq 20\lambda \sim L$, while far beyond this threshold, $\xi \simeq \lambda \ll L$, which corresponds to the observed regime of spatiotemporal chaos. Ning *et al.* [28] investigated rotating Rayleigh-Bénard convection in a parameter region where the Küppers-Lortz instability produces spatiotemporally chaotic dynamics at the onset of convection. They found that the time-averaged convection patterns showed ordered structure which displayed the symmetry of the container. They explained that the forcing at the boundary of the container pins the phase of the pattern there, resulting in

a phase rigidity of the pattern which manifested itself in the temporal averages. They studied the correlations between the instantaneous patterns and the averaged regular pattern, and showed that fluctuations in the spatial structure of the pattern were correlated with fluctuations in the total heat flux through the layer.

STC has also been studied in Faraday surface waves. Under periodic vertical motion, the free surface of a fluid layer is unstable to standing surface waves. This kind of instability was first reported by Faraday in 1831 [29]. There is a large literature on the Faraday instability ([30] [38]). Here we focus on recent work relevant to the study of STC. A statistical analysis of the transition to spatiotemporal chaos in Faraday waves at moderately high aspect ratio ($\Gamma = 50 - 100$, where Γ is defined as the ratio of the lateral cell dimension L to the wavelength λ of the surface waves) was reported by Tufillaro *et al.* [1] Another approach to detecting the transition to spatiotemporal chaos in the Faraday instability was taken by Ciliberto *et al.* [39], who statistically analyzed the fluctuations in the vertical acceleration which drives the motion of the fluid layer.

Recently, Gluckman *et al.* studied STC in the Faraday instability extensively using a number of statistical measurements [9][13]. They found structured time average patterns which had an ordered spatial structure in a large thin layer system [13]. They found the time averaged patterns were aligned with respect to the walls of the container. The amplitude of the average surface wave pattern, determined from optical measurements, was observed to be dependent on the degree to which

the surface wave's phase was pinned at the lateral boundaries, and to decrease with increasing drive amplitude. They also measured the correlation length of the pattern from the decay of the spatial autocorrelation function to estimate the degree of disorder in the instantaneous pattern.

1.3 Related work on the Printer's Instability

The printer's instability (also called directional viscous fingering) is an instability of the meniscus of a viscous fluid confined in a gap of varying width, between two moving solid surfaces. It occurs often in industrial coating processes. The primary motivation for much of the early work on the printer's instability has come from coating applications. This is because instabilities that arise when a thin layer of fluid is spread or coated onto a surface lead to an uneven coating thickness, often called ribbing, which is generally undesirable. It was first described by Pitts and Greiller [40] and Taylor [41].

Over the last thirty years, there has been a substantial amount of research on this system and related instabilities ([40] [50]). Recently, the ideas of nonlinear dynamics have been applied to problems in coating [51]. Rabaud *et al.* studied the fingering patterns produced in the printer's instability, both theoretically and experimentally [17] [54].

Recently, Pan and de Bruyn investigated the traveling-wave state in this system ([55] [58]). The work reported in this thesis is an extension of their research.

The experimental set-up of the printer's instability consists of two horizontal cylinders, which are parallel, but vertically offset, one inside the other, such that the gap b_0 between the cylinders is smallest at the bottom. A cross section through the two cylinders is shown in Fig 1.2. In this experiment, b_0 was fixed at 0.110 ± 0.001 mm. A quantity of viscous fluid, sufficient to keep the bottom part of the gap between the cylinders filled, is introduced into the gap. The velocities of the two cylinders are controlled by two computer-controlled motors, and form two independent control parameters controlling the finger patterns and the transition to chaos. Depending on the sense and speed of the rotation of the two cylinders, fingering patterns with different dynamical behavior develop at the meniscus. For example, with one cylinder rotating, a stationary finger pattern appears at the meniscus, and with both cylinders rotating, different time dependent patterns are observed, depending on the direction and speed of the two cylinders. The patterns observed over a range of velocities of the two cylinders are indicated in the dynamical phase diagram of the meniscus, Fig. 1.3. Typical interface patterns are shown in Fig 1.1. These include a stationary periodic pattern of symmetric fingers (Fig. 1.1(a)); a traveling-wave pattern consisting of asymmetric, traveling fingers which occurs for counter-rotating cylinders (Fig. 1.1(b)); solitary traveling waves in the form of localized patches of asymmetric fingers propagating through a background of stationary fingers (Fig. 1.1(c)); and spatiotemporal-temporal chaos, which occurs for co-rotating cylinders, in which the system exhibits chaotic dynamics, characterized

by a loss of spatial and temporal coherence of the cellular pattern (Fig. 1.4(d)).

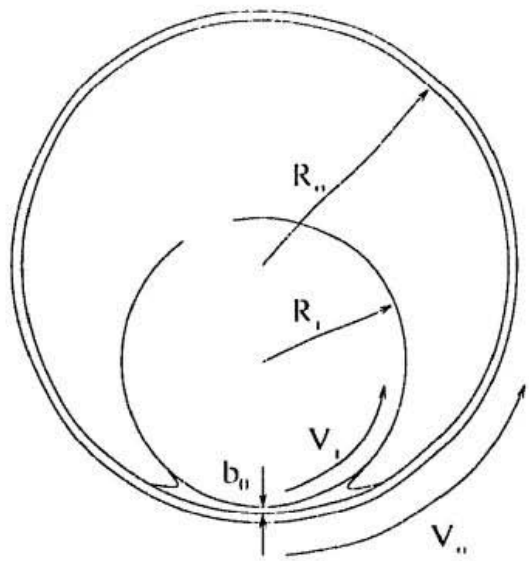

Figure 1.2: Sketch of a cross-section of the experimental system, where b_0 0.110 1 0.001 mm.

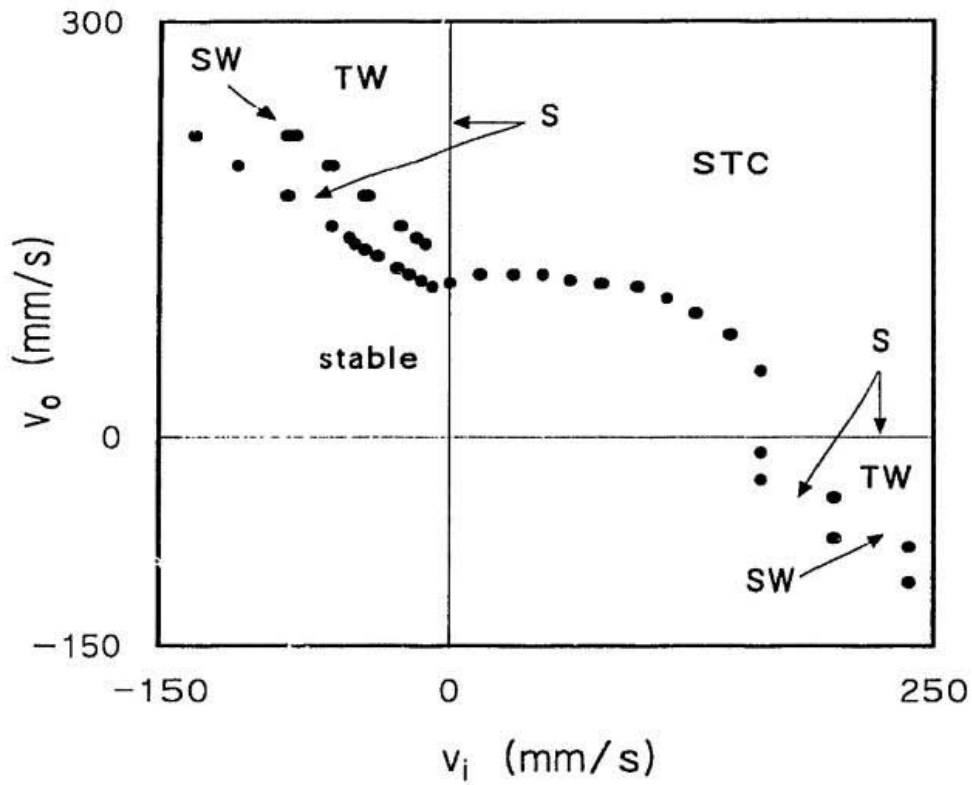

Figure 1.3: Dynamical phase diagram of the interface, in terms of the rotation speeds of the two cylinders. S - stationary fingers; TW - traveling waves; STC - spatiotemporal- temporal chaos; SW - solitary waves. From Ref. [58]

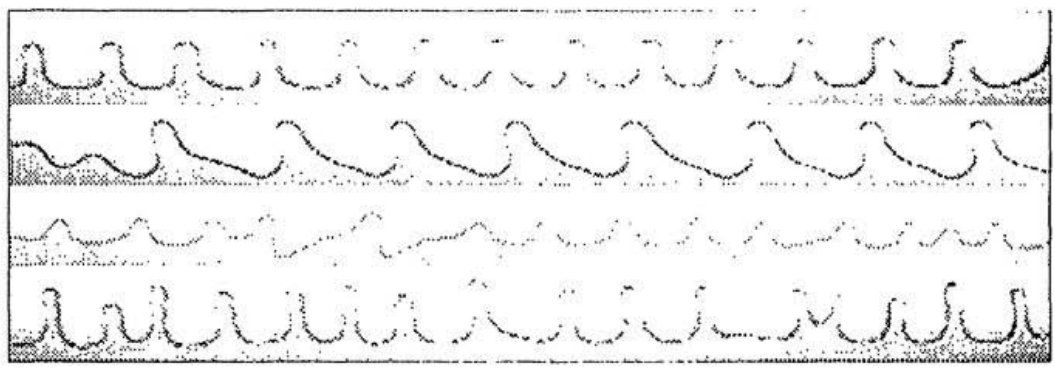

Figure 1.4: Examples of patterns observed at the oil air meniscus in the experiment of printer's instability. From top to bottom: Symmetric, stationary fingers; asymmetric fingers drifting to the right; solitary wave traveling in a background of stationary fingers; spatiotemporal chaos. From Ref. [58]

The work of Pan and de Bruyn mainly concerned studies of the stationary and traveling wave patterns, which occur on the axes, and in parts of the second and fourth quadrants of Fig. 1.2. Measurements of the onset and development of the stationary finger pattern were made which indicated that finite-size effects delayed the onset of the fingering instability in their experimental system. They also observed a supercritical parity-breaking transition, at which the stationary pattern lost its reflection symmetry and began to drift along the meniscus. They found that the asymmetry increased with the square root of the control parameter, and that the drift velocity was linear in the asymmetry, in agreement with theoretical predictions ([59] [61]).

It has been observed that stationary patterns can evolve into STC through STI. The STI state in the printer's instability was investigated by Michalland and Rabaud [62]. It occurs along the edge of the STC region indicated on Fig. 1.2. Dilatation waves and asymmetrical pairs of cells were observed in the spatiotemporally intermittent regime, and possible reasons for such phenomena were given. Michalland *et al.* [63] also presented a statistical description of the transition to spatiotemporal chaos in the printer's instability. They investigated the transition to chaos by measuring the fraction of the pattern which was chaotic, the distribution of the widths of ordered domains and the distribution of lifetime τ of ordered behavior at a spatial point. They found that the mean chaotic fraction increased with the increase of their control parameter Ca_o (the capillary number of outer

cylinder). They found, for Ca_v in the range 0.015 to 0.03, that the distribution of the widths of the ordered domains can be fitted by a decaying exponential. The e-folding distance L (the slope of the exponential decay) was treated as the characteristic width of the ordered areas. The ratio $(\lambda/L)^2$, where λ is the wavelength of the pattern, increased linearly with Ca_v. From this graph, they found the value of Ca_v at which L diverged, $Ca_v = 0.011 \pm 0.001$, and took this value as the threshold of STI transition. Near this threshold, the distribution of the widths of the ordered domains decreases algebraically, rather than exponentially. Similar behavior was found in the distribution of temporal durations.

There has been little work done on the STC state in the printer's instability itself. The statistical studies of Gluckman [9] and his collaborators on STC in the Faraday instability encouraged us to use the same techniques to study the STC region of the printer's instability. Relative to fully three or two dimensional pattern forming systems, a system such as the printer's instability which forms one dimensional patterns has the advantage of simplicity. The study of various statistical properties, including time averages and correlation functions, can be used to help characterize and to understand the STC state. In this work, we studied the long time average of the STC pattern, and using the cross-correlations between instantaneous 1 D images we studied how correlations decay with time. By varying the averaging time we studied how the averaged pattern approaches its long time average. Using spatial autocorrelation function we determined the correlation length of the pattern,

which gives a quantitative measure of the spatial coherence in the STC state. We also study the effect of the control parameter Ca_s on the behavior of ξ.

Chapter 2

Experimental Methods

2.1 Apparatus

The experimental set-up is shown schematically in Fig. 2.1. The apparatus consists of two horizontal cylinders, mounted one inside the other, but off centered, with the gap between the cylinders smallest at the bottom. A cross section through the two cylinders is shown schematically in Fig. 1.2. The outer cylinder is transparent and made of Plexiglas. It rested on four bearing-mounted rollers. It has an inside radius $r_o = 66.7$ mm and a length $l_o = 210$ mm. The inner cylinder is made of white Delrin and mounted on an axle which is supported by bearings. It has radius r_i 21.85 mm and length $l_i = 202$ mm. A small amount of silicone oil, enough to keep the gap region flooded during the experiment, is poured into the gap between the cylinders. The experimental fluid is confined by annular end caps attached to the outer cylinder. The oil used in the experiment was obtained from Aldrich Chemical Co. (catalog no. 14,615-3). It had viscosity $\mu = 0.525$ g/cm s, surface tension σ 19.4 g/s^2, and density $\rho = 0.963$ g/cm^3 at room temperature. As illustrated in Fig. 2.1, the z positions of the ends of inner cylinder can be independently adjusted with micrometer screws, as well as the y position of the outer cylinder. The x positions of

both inner and outer cylinders can also be adjusted. The driving belts, running on a pulley on the axle of the inner cylinder and a groove on the outer surface of the outer cylinder, connect the cylinders to two computer-controlled microstepping motors (Compumotor Plus, CPLX 57-120) which rotate the two cylinders independently. This arrangement is illustrated in Fig. 2.1. A 80286-based personal computer, which is interfaced to the motors by an RS-232 serial line, is used to control the speeds of the motors and to collect experimental data. The rotation frequency of the motors could be controlled with a resolution of 0.001 Hz. Taking into account the pulley ratios, the minimum velocity increment for both cylinders was 0.01 mm/s.

The oil air menisci are linear and parallel to the cylinder axes when the cylinders are at rest. When the cylinders rotate fast enough, the front meniscus, *i.e.*, the meniscus towards which the fluid is pulled, becomes unstable. Depending on the speeds and directions of rotation of the inner and outer cylinders, various one-dimensional fingering patterns can appear on the meniscus. Typical fingering patterns are shown in Fig. 1.3. The capillary number is defined as $Ca = \mu V/\sigma$, where V is the velocity of cylinder, μ is the viscosity of the oil and σ the interfacial tension. We use Ca_i and Ca_o as the two control parameters of the experiment, where Ca_i and Ca_o refer to the inner and outer cylinders, respectively. When the two cylinders are co-rotating, a chaotic fingering pattern appears on the meniscus as illustrated in Fig. 1.3 (d). The threshold for STC depends on the geometry of the apparatus (*i.e.*, on b_0, the minimum spacing between the two cylinders, and the radii of the

cylinders) and on the two capillary numbers.

Fig. 2.2 is a block diagram of the experiment. Images of the chaotic air oil meniscus were recorded using a Charge-Coupled Device (CCD) video camera (Pulnix TM-7CN) and monitor (Burle TC 1910A), and stored on the personal computer using a video frame grabber (Imaging Technology, Inc. PCVISION plus) capable of grabbing 30 frames per second.

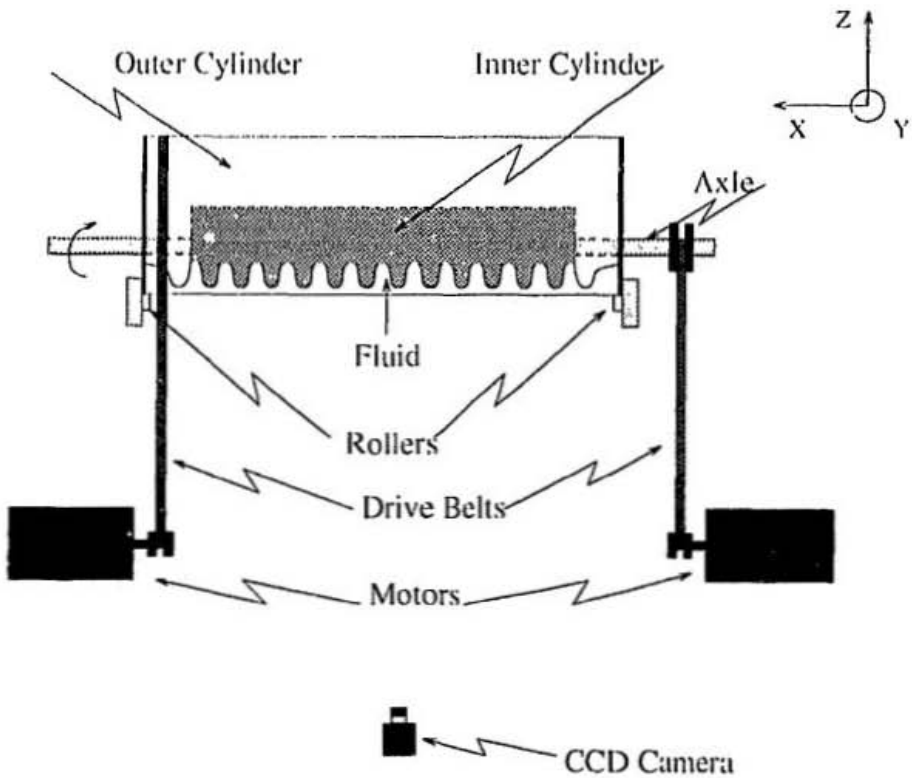

Figure 2.1: Schematic drawing of the experimental apparatus with only the inner cylinder rotating

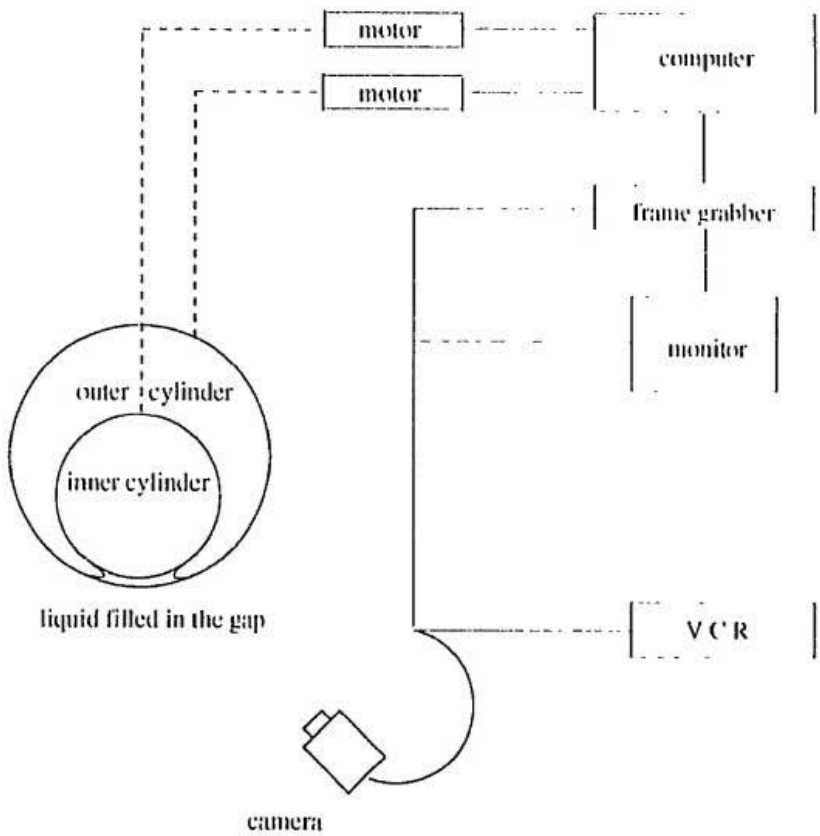

Figure 2.2: Block diagram of the experimental apparatus.

2.2 Acquisition and Presentation of Video Data

Of particular interest in our experiment is the disordered fingering pattern shown in Fig. 1.3(d). The dynamics of such a pattern can be visualized through a so-called spatiotemporal image. By recording the intensity of one horizontal video line through the finger pattern at times separated by constant time intervals, a spatiotemporal image can be constructed. A typical spatiotemporal image obtained in our experiment is presented in Fig. 2.3. In this figure, time increases downwards and position varies along the horizontal axis. The dark lines indicate the tracks of the edges of the oil fingers. Variations in the background intensity, due to the variations of the illumination in space and with time, are visible in Fig. 2.3. These interfere with qualitative analysis of the image, and make quantitative analysis all but impossible. To eliminate background variations, we record a background image of the appropriate video line with no pattern present. We then calculate the mean intensity of that background, and of each line in spatiotemporal image. At each time, the background is scaled by $W(\Delta t)$ as defined below and subtracted from the image such that the difference has zero mean. The resulting image is shown in Fig. 2.4. The background is now uniform in space and time. Mathematically, if we denote as $I(x, \Delta t)$ and $I_b(x, \Delta t)$ the intensities along a line of the image and the background, respectively, then background subtraction can be written as

$$I_{bs}(x, \Delta t) = I(x, \Delta t) - I_b(x, \Delta t) * W(\Delta t), \tag{2.1}$$

where $W(\Delta t) = \overline{I(x,\Delta t)}/\overline{I_b(x,\Delta t)}$ is the weight for the subtraction and varies with time. Here x is the position coordinate, Δt is the time, and the overbar represents an average over space. The original image contains 640 pixels in the x direction, but the computations include only the central region $L/4 \leq x \leq 3L/4$ along the spatial domain of the image. This region contains all moving fingers in our experiment. The constant time interval (between two adjacent lines) along the y axis in Fig. 2.4 is 0.05 sec, which is the minimum interval possible with our imaging system. Except at high cylinder speeds, when the motion of the fingers is rapid and highly chaotic, this time interval is sufficiently short compared to the time scale for motion of the fingers, so that the spatiotemporal images can adequately display the spatiotemporal dynamics of the patterns under study. In Fig. 2.4, the narrow light gray regimes are the fingers, and the wide gray regimes are the nodes between fingers.

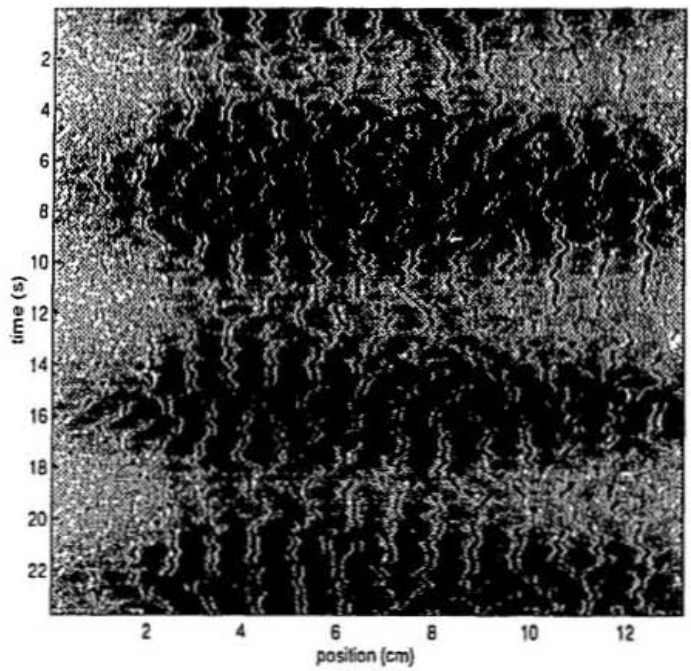

Figure 2.3: Spatiotemporal image of a chaotic pattern in the printer's instability. Time increases downward, and the horizontal coordinate is position. The total time shown is 24 s, and the central 13.2 cm of the experimental system is shown.

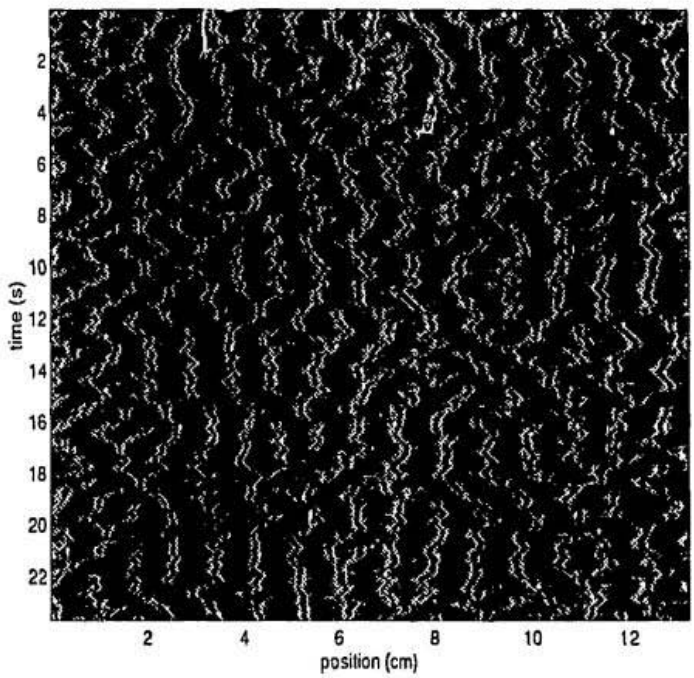

Figure 2.4: The spatiotemporal image of Fig. 2.3 with background subtracted as described in the text.

Chapter 3

Experimental Results and Statistical Analysis

3.1 Introduction

In this work, we focus on a statistical analysis of the fingering pattern and its dynamics in the spatiotemporal chaos region. We fixed the inner capillary number Ca_i at $Ca_i = 0.609$, which is above the threshold at which the stationary fingering pattern first appears. Our control parameter for the transition to chaos is the capillary number Ca_o of outer cylinder. At $Ca_o = 0$, the meniscus shows a pattern of stable fingers. We then set the outer cylinder rotating in the same sense as the inner cylinder. In order to avoid transient effects in this and all other data presented in the thesis, we waited about 20 minutes after a change of Ca_o before taking data. Figs 3.1–3.3 present typical spatiotemporal images recorded at different values of Ca_o, and show different dynamics. In all these three images, the x axis corresponds to position along the apparatus and the y axis is time. For very low values of Ca_o, the stationary fingering pattern remained stable. When Ca_o reached about 0.005, disordered patches started to appear occasionally on the ordered background pattern, as shown in a spatiotemporal image in Fig. 3.1. This kind of behavior was observed in a range of Ca_o values from 0.005 to 0.07. The spatiotemporal images in

this range of Ca_v values show that laminar (*i.e.*, ordered) domains are dominant, and the chaotic (*i.e.*, disordered) domains are fluctuations which develop in a laminar background. As Ca_v is increased, the disordered patches become more and more frequent, and start to spread both spatially and temporally. For Ca_v between 0.082 and 0.16, chaotic fingers become the dominant feature of the pattern. Fig. 3.2 is a typical spatiotemporal image from this regime. In this case, laminar domains can be viewed as fluctuations in the chaotic background. The dynamics of the pattern for $0.005 \lesssim Ca_v \lesssim 0.16$ are referred to as STI. STI is an intermediate state between the stable, stationary pattern and the fully chaotic state. Finally, when Ca_v was high enough (above 0.165), the interface has everywhere lost its spatial and temporal coherence, as shown in Fig. 3.3, and is in a state of spatio temporal chaos (STC).

To summarize, we can describe the spatiotemporal dynamics of the 1D fingering patterns by two different stages: the first stage is STI, for $0.005 \lesssim Ca_v \lesssim 0.16$, in which chaotic and laminar regions coexist in space and time, at 1 the second is STC, for $Ca_v \gtrsim 0.165$, in which chaotic fingers spread over the whole spatiotemporal domain.

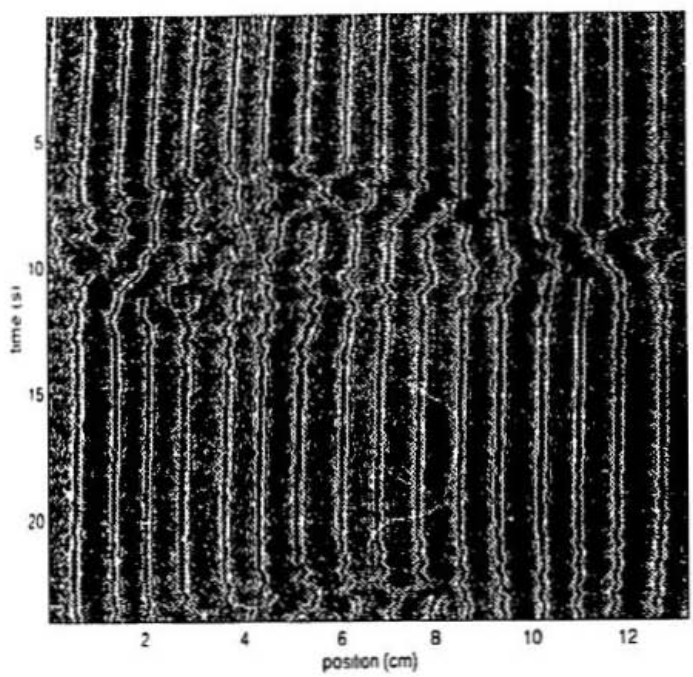

Figure 3.1: The central region of a spatiotemporal image with $Ca_u = 0.0491$: chaotic domains appear and disappear in a laminar background. The horizontal axis is position (space) and the vertical axis is time.

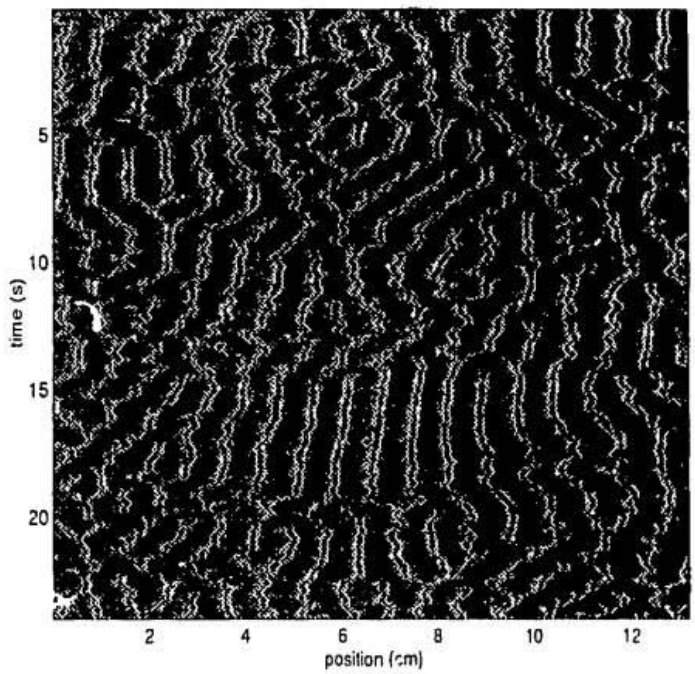

Figure 3.2: The central region of a spatiotemporal image with Ca_t 0.1398; laminar domains appear and disappear in a chaotic background.

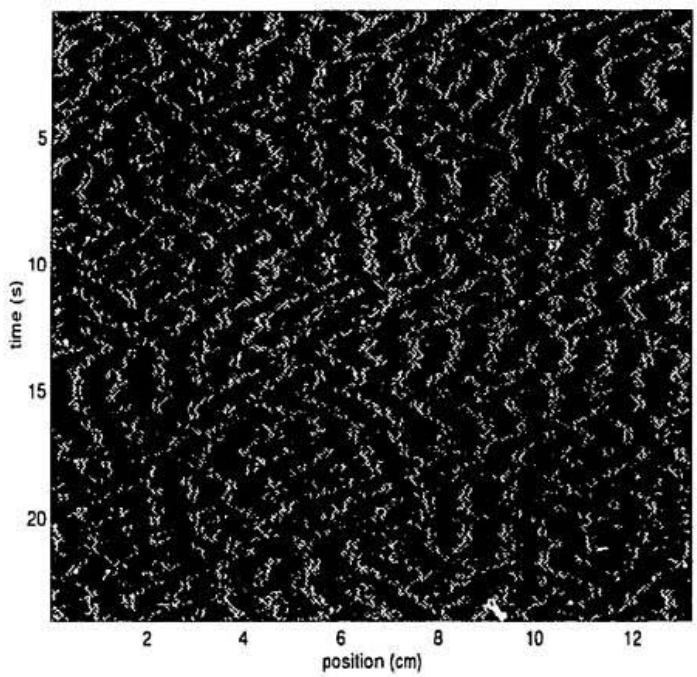

Figure 3.3: The central region of a spatiotemporal image in the spatiotemporally chaotic state with $Ca_{\perp} = 0.4113$.

3.2 The time-averaged image

As mentioned before, with only the inner cylinder rotating, stationary fingers are obtained. With the two cylinders corotating, chaotic finger patterns appear. We studied these chaotic patterns by looking at the long-time average pattern. The background was subtracted from 1D instantaneous images as described in section 2.2. We first show the instantaneous long time average intensity of patterns obtained in the stationary finger state. The 1D background-subtracted instantaneous fingering pattern and its average over a time long compared to the characteristic time of fluctuations are presented in Fig 3.4, for $C'a_i$ fixed at 0.609 and $C'a_o$ equal to zero. In the same way, we got the instantaneous chaotic fingering pattern and its long time average presented in Fig. 3.5, for both $C'a_i$ and $C'a_o$ equal to 0.609. The long time averages in both Fig. 3.4 and Fig. 3.5 were obtained by averaging over 15000 individual 1D video lines through the patterns, over a time of 12.5 minutes.

The time-averages of the two patterns are totally different. As expected, the time average of the stationary finger pattern has the same spatial structure as the instantaneous pattern, but with much less noise. On the other hand, the time average of the chaotic pattern shown in Fig. 3.5 has no spatial structure at all. This result is not entirely surprising, as the average of a random variable is expected to be zero. However, this result is different from what has been seen in other experiments. Recently, it was observed in experiments on 2D spatiotemporally chaotic patterns in rotating Rayleigh-Bénard convection [28] and the Faraday instability [9]

that the time-averaged patterns had spatial structure, the symmetry of which was determined by the symmetry of the boundaries. Gluckman *et al.* [9] also observed that the amplitude of the structure in the average image decreases with increasing phase fluctuations resulting from an increase in their drive acceleration, and depends on the degree of phase pinning at the boundaries.

Now we turn to a qualitative discussion of the reasons for the structureless long time average in the chaotic state. Ideally, the instantaneous patterns can be regarded as being built on a single wavenumber base pattern. If the phase of the pattern is pinned at the boundary, as would happen with solid side walls, the phase of the instantaneous 1D fingering pattern is expected to be coherent in t, so the long time average will have a structure. On the other hand, if waves can freely change phase at the boundaries, a structureless long-time average is expected, as observed in [9]. In our experiment, the boundaries can be considered to be "soft" boundaries because no rigid walls exist at the ends of the meniscus, so the phase of the instantaneous wave pattern varied freely at the ends. Thus phase coherence was lost spatially and temporally. The result of the random phase fluctuations is that the superposition of the instantaneous chaotic patterns leads to a zero time average. We noticed that, compared to the phase fluctuations, amplitude fluctuations are small. Thus we assume that amplitude fluctuations did not affect the basic structure of the long time average. The rms deviation of the long time average is roughly 1/10 that of the instantaneous one, and this magnitude is well within noise level as shown in

Fig 3.5 (b). It was also observed that local spatial nucleation and collision of fingers happened from time to time. These local activities could cause local dislocation and disclination of fingers, and therefore, contribute to the zero mean amplitude of the long-time average patterns. It was also found that for higher values of the capillary number Ca, a structureless average could be obtained in a shorter time.

In conclusion, the structurelessness of the long time averages of the instantaneous fingerings patterns in the STC regime was caused by phase variations in the instantaneous fingering patterns. Phase pinning at the boundaries is not important due to the soft boundary condition at the ends of the system.

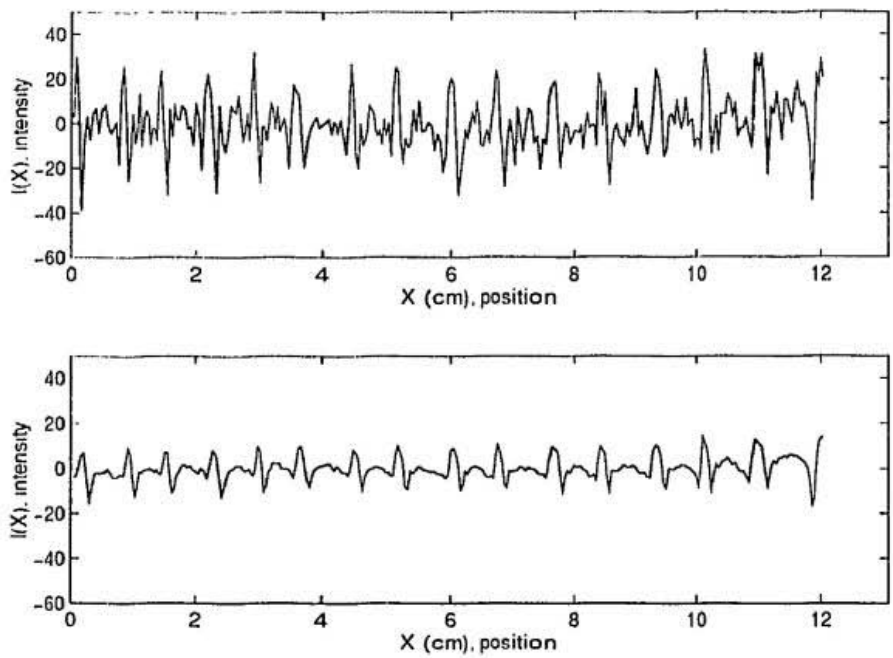

Figure 3.4: The background subtracted instantaneous and long time averaged intensity patterns for the stationary finger state, at $Ca_i = 0.609$ and $Ca_o = 0$.

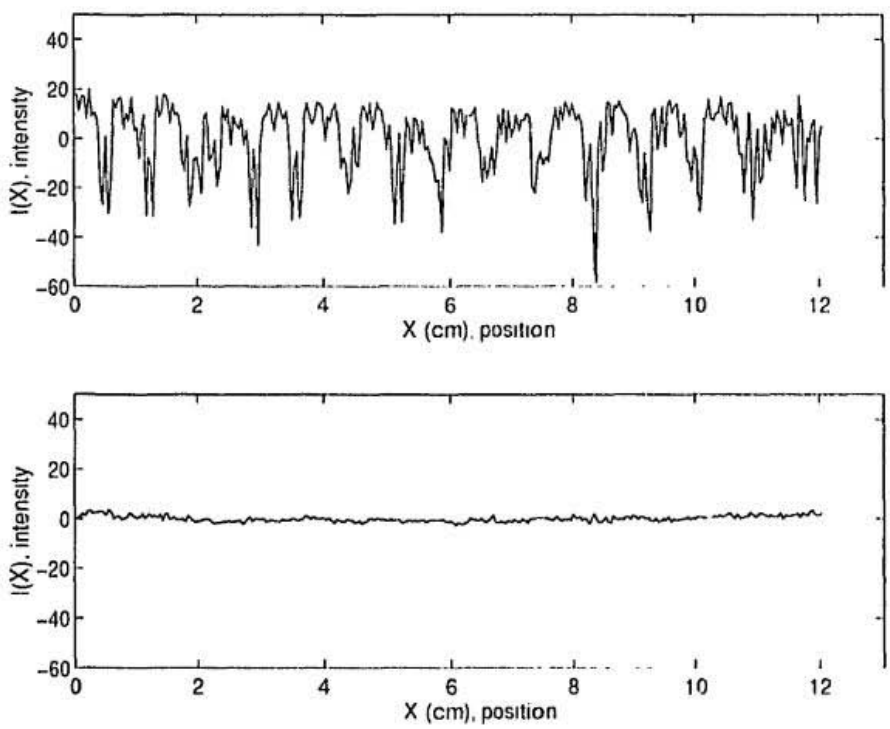

Figure 3.5: The instantaneous and long time averaged intensity patterns for a chaotic finger pattern, at $C'a_t = 0.609$ and $C'a_{av} = 0.280$.

3.3 The approach to the infinite-time average

It is interesting to probe the way the average pattern approaches the infinite time average as the averaging time is increased. The way the average pattern approaches the infinite time average really tells us how fast temporal coherence is lost. Motivated by such considerations, we measured the rms deviations of finite time averages from the infinite time average. We define the rms difference between finite and infinite time averages as:

$$D(\tau) = \langle (A(x,\tau) - A(x,\infty))^2 \rangle^{1/2} \tag{3.1}$$

where $A(x,\tau) = (1/\tau)\int_0^\tau I(x,\tau)d\tau$. The angle brackets denote an average over space. $D(\tau)$ would decay as the inverse square root of the integration time for a system with random Gaussian fluctuations. $D(\tau)$ is plotted on a log-log graph in Fig. 3.6. for $Ca_n = 0.197$. For $t < 50$ s, the data approximately obey a power law with exponent $\beta = -0.47 \pm 0.02$. This indicates that for short averaging times (i.e., less than about 50 s) the short time average approaches the long time average approximately like a Gaussian variable. However, for $t < 100$ s, β is -0.43 ± 0.02. The fact that the magnitude of the slope is below 0.5 for longer averaging times indicates that the time correlations decay more slowly than a Gaussian variable. As seen from Fig. 3.6, $D(\tau)$ fluctuates quite a lot at large τ. Ideally, the infinite time average should approach to zero as it is structureless. However, the actual infinite long time average is not exactly zero due to noise involved, and the subtraction of two long time averages would bring in noise and make data fluctuate at the tail.

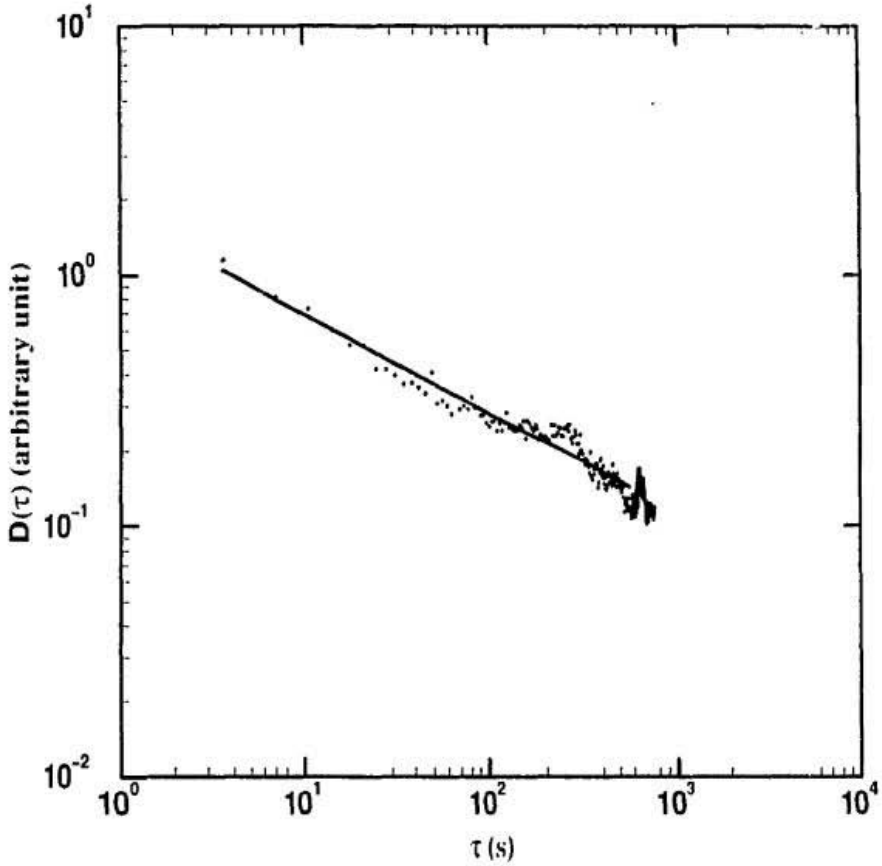

Figure 3.6: A log-log plot of the rms deviation of the short time average from the long time average at $Ca_a = 0.329$. For short averaging times ($t < 50$ s), the time average approaches the long time average much like a Gaussian, but for longer averaging times the decay is slower.

3.4 Time-dependent cross-correlation coefficient

In order to probe the time correlation among the instantaneous 1D images, we calculated the cross correlation coefficient between the spatial fluctuations in the instantaneous images as a function of time. We call the instantaneous 1D image $I(x,t)$. $I(x,0)$ is the image recorded at time zero, and we denote by G_{cc} the cross-correlation coefficient defined as:

$$G_{cc}(t) \equiv \frac{\langle \delta I(x,0)\delta I(x,t)\rangle}{\delta I(x,0)_{rms}\delta I(x,t)_{rms}} \tag{3.2}$$

where $\delta I(x,t) = I(x,t) - \langle I(x,t)\rangle$ represents the subtraction of the spatial mean, and the brackets denote an average over space. The correlation coefficient lies between -1 and 1. The correlation coefficient will be zero if two instantaneous images are completely uncorrelated, and will be 1 if they are perfectly correlated (*i.e.*, if they are identical). Typically, G_{cc} was calculated from a series of 450 instantaneous images recorded 0.05 s apart. For each such 1D instantaneous image, we consider only the central region $L/4 < x < 3L/4$ as this region is where all fingering patterns occur.

As mentioned at the beginning of this chapter, STC can be reached by passing through a state of spatiotemporal intermittency. For a complete study, we have investigated the early time decays of G_{cc} of both STI and STC.

At very low outer cylinder speeds, G_{cc} decays exponentially at early times. Fig. 3.7 is a graph of G_{cc} as a function of t for $Ta_o = 0.049$. The same data for small time are shown in Fig. 3.8 and on a semi-log graph in Fig. 3.9. The decay of G_{cc}

in this region can be fitted by an exponential decay, $G_{\tau\tau} \propto e^{-\alpha t}$, with decay rate $\alpha = 0.50 \pm 0.03\ s^{-1}$, as shown in Fig. 3.9. A power law fit, shown as the dashed line, was also tried for the data in Fig. 3.9, but did not describe the data as well.

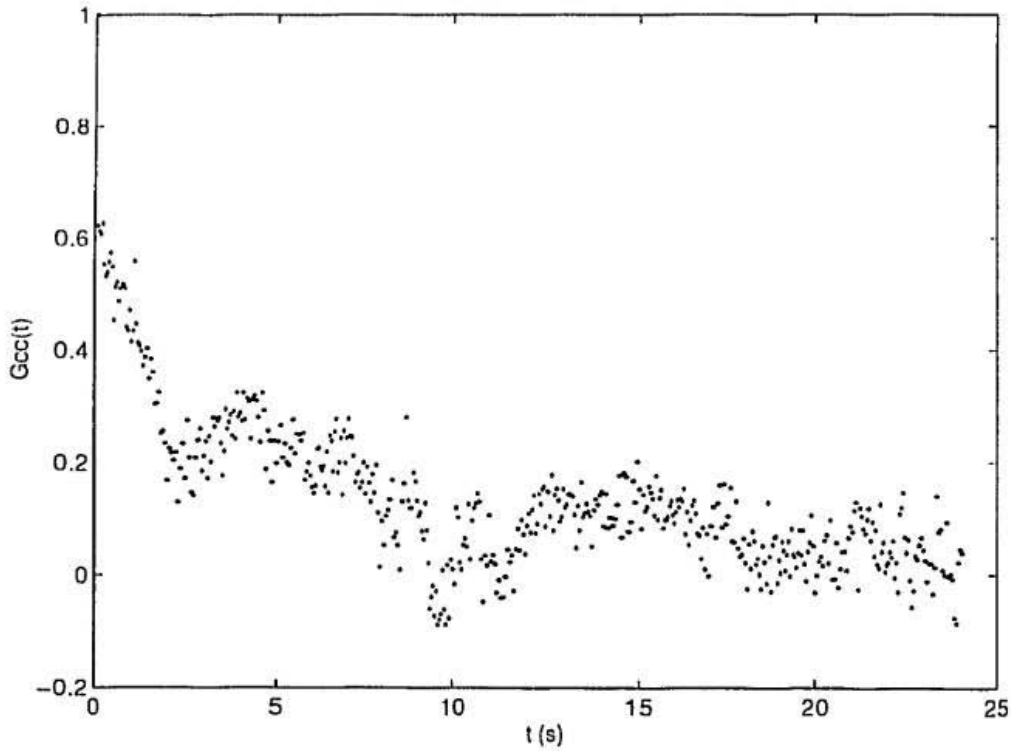

Figure 3.7: The time-dependent cross-correlation coefficient at $Ca_0 = 0.049$.

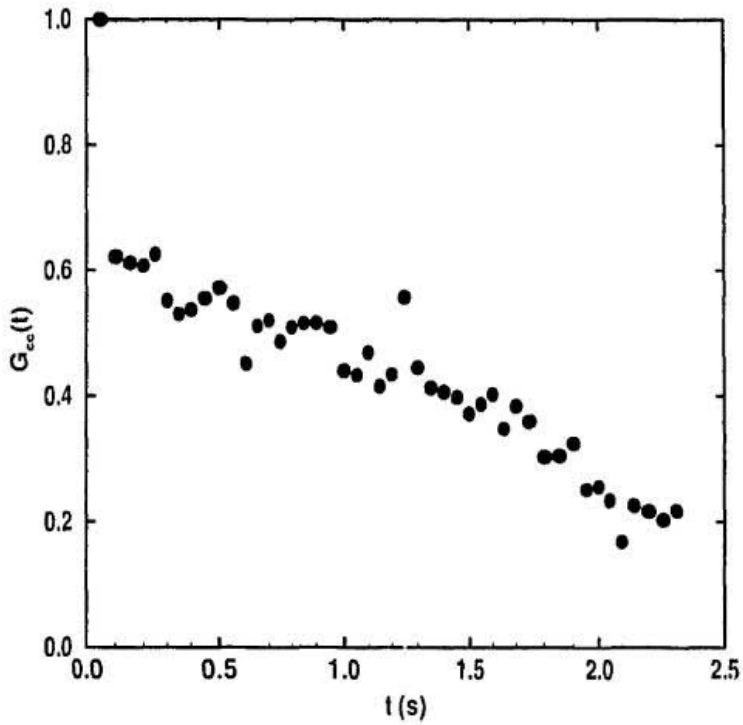

Figure 3.8: The early time decay of the G_{cc} data shown in Fig. 3.7.

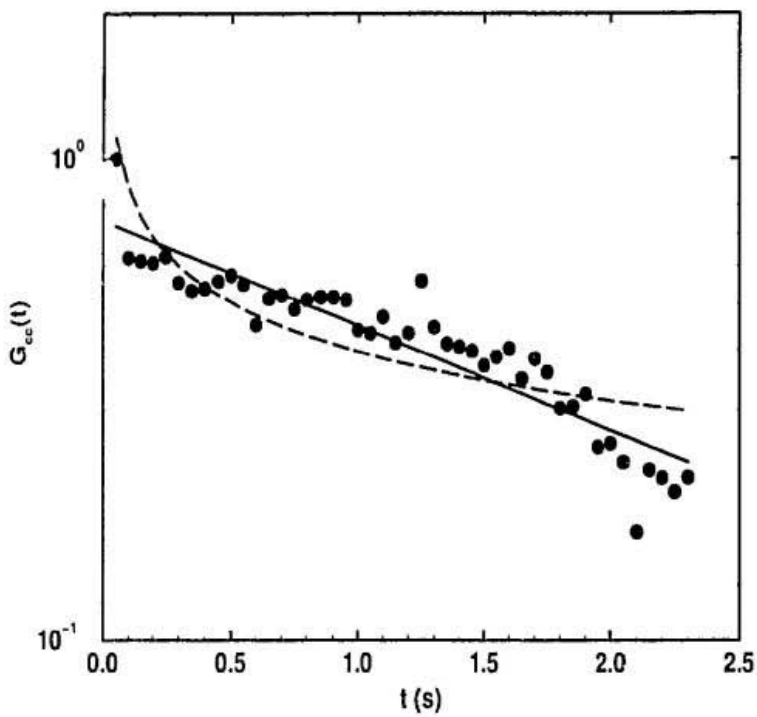

Figure 3.9: A semi-log plot of the data shown in Fig. 3.8. The data can be described by an exponential decay with decay constant $\alpha = 0.50 \pm 0.03$ s^{-1} shown by the solid line, but not by a power law decay, as the dashed line shows.

Both power law and exponential decays were fitted to the early time G_{xx} data for a number of values of Ca_{tt}. Generally, the exponential fits described the data better, as indicated by the values of the χ^2 obtained from the fits. Figure 3.10 shows the decay constant α as a function of Ca_{tt} for two sets of data taken at the same value of Ca_{rr}. α increases with Ca_{tt}, indicating that the correlations decay more quickly as the system becomes more chaotic, as expected. For Ca_{tt} higher than 0.100 the system is highly chaotic, and the early time decay of G_{xx} could not be observed. Indeed, in the STC regime, the time correlation between instantaneous images decreases so fast that few data can be selected for study. Therefore, only the regime close to the onset of STC could be investigated.

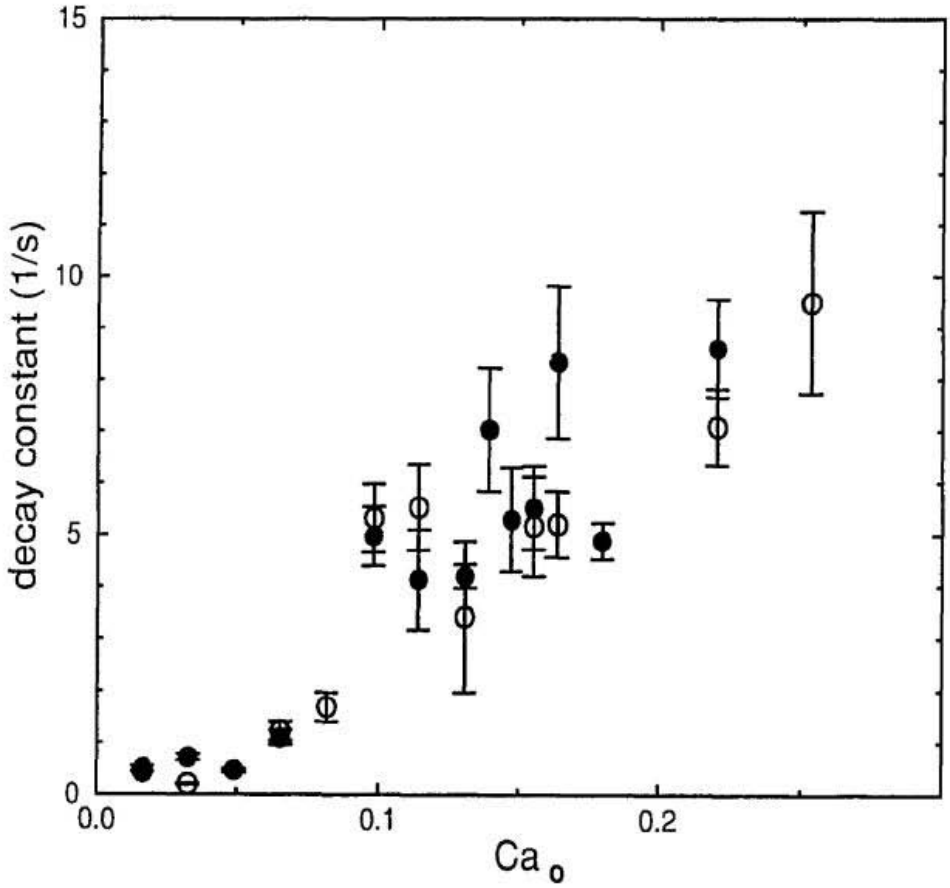

Figure 3.10: The decay constant obtained from exponential fits to the early time decay of G_{xx} as a function of Ca_o. The two symbols are from two different sets of data taken at the same value of Ca_i.

It is worth mentioning how the early-time G_{ss} data were selected. G_{ss} is initially high, but then decays to random noise. The range of data which lie above noise level at early times could be found using the Matlab statistics function *Normplot*, which produces a Gaussian probability plot of the data. The original purpose of this function is to allow graphical determination of whether a set of data could come from a normal distribution. If the data are normal the plot will be linear. For other distributions, curvature in such a plot can be expected. In our case these plots provided a criterion to distinguish the early time decay data from long time fluctuations, which were Gaussian. Fig. 3.11 shows G_{ss} as a function of t for Ca_n 0.222, which is in STC region. We can see $G_{ss} < 0.2$ except for the data at the early time. So the long time fluctuations of G_{ss} are Gaussian. A Gaussian probability plot of the data in Fig. 3.11 for $Ca_n = 0.222$ is shown in Fig. 3.12. From Fig. 3.12, we see that for $G_{ss} \lesssim 0.2$ the data follow a Gaussian distribution, but the data higher than 0.2 obviously do not. In Fig. 3.12, we only used the data above 0.2 at the early time for analyzing the behavior of early time decay. For different Ca_n, we used this method to decide the range of the data for G_{ss} at each early time decay. For $Ca_n > 0.40$, the early time decay was too fast to be observed with our time resolution, which was 0.05 second. This can be seen in Fig. 3.13 which is a Gaussian probability plot for data taken at Ca_n =0.411. Almost all of the data lie on the line expected for Gaussian noise.

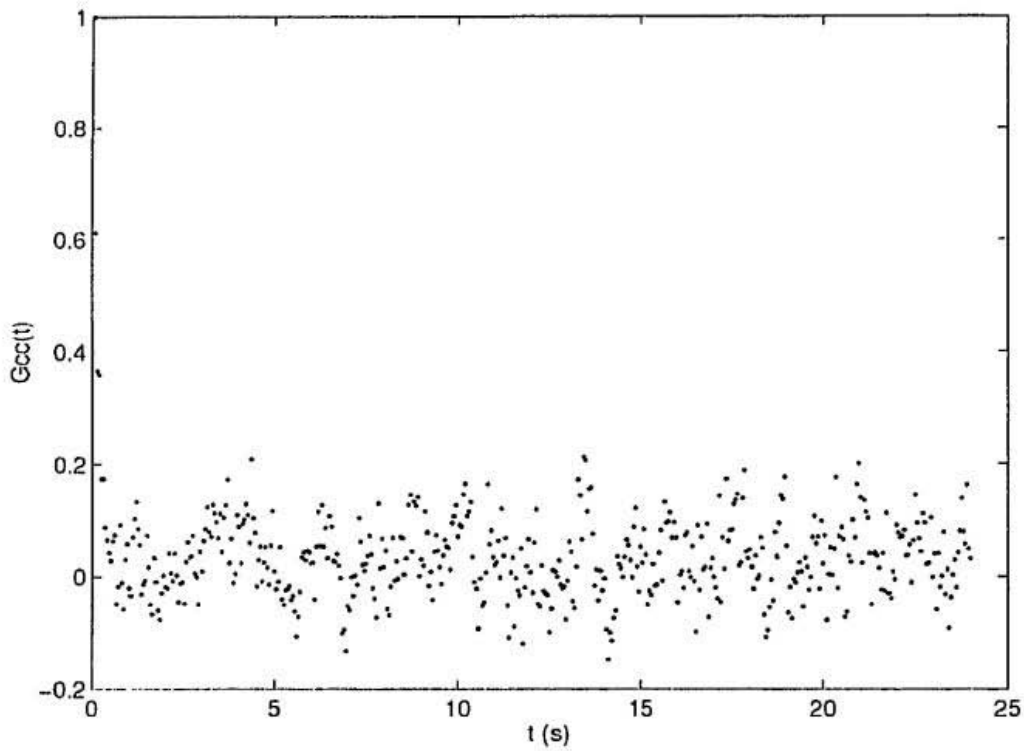

Figure 3.11: The time-dependent cross-correlation coefficient in deep STC, where $Ca_c = 0.222$.

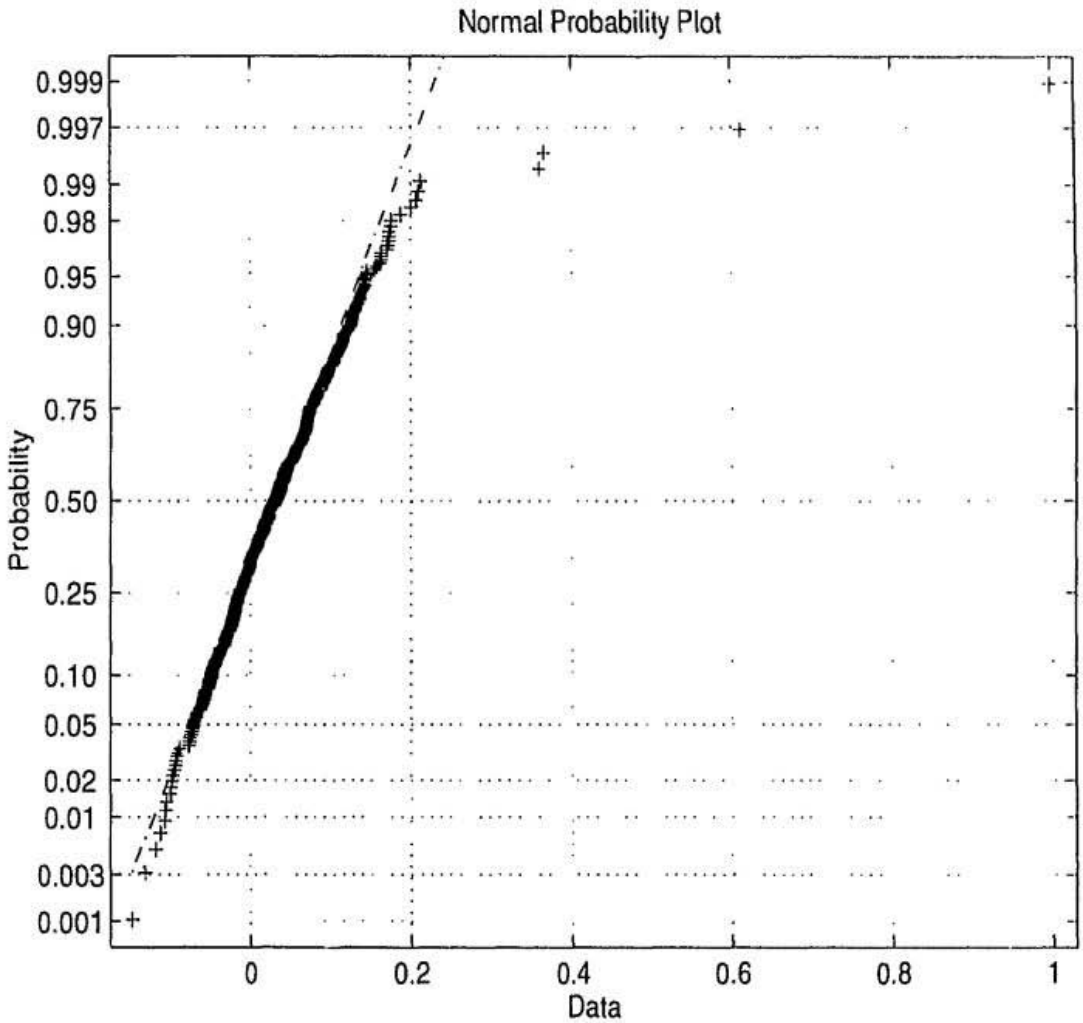

Figure 3.12: The Gaussian probability plot for the G_{cc} data shown in Fig. 3.11, at $Ca_0 = 0.222$. Data fitted by the dashed line can be described by a Gaussian probability distribution. The data at $G_{cc} > 0.2$ are obviously not Gaussian. Although the G_{cc} at early time decay rapidly to noise level, we can still select $G_{cc} > 0.2$ to analyze the behavior of the early time decay.

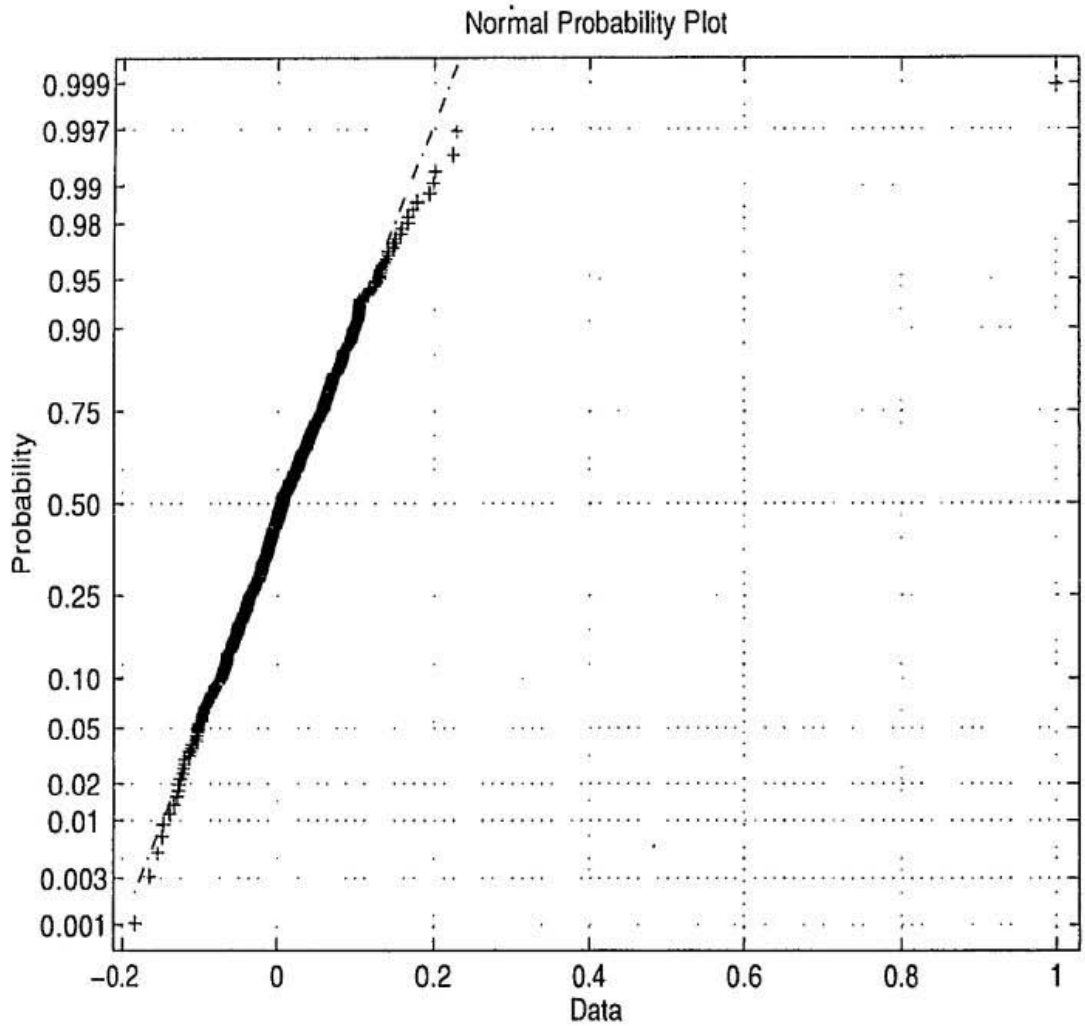

Figure 3.13: The Gaussian probability plot of C_{cc} for $Ca_o = 0.411$. For data fitted by the dashed line, their probability distribution will be Gaussian. Almost no data lie above the noise.

We found there was usually a high fluctuation in G_{yy} (see Fig. 3.7) for instantaneous 1D images in the state in which chaotic patches developed in a laminar background (refer to section 3.1). This is understandable because the chaotic domains are limited in spatial and temporal extent, so the basic fingering patterns were correlated at some times and uncorrelated at other times. This caused the obvious fluctuations in G_{yy}. On the other hand, relatively small fluctuations were observed when the pattern was totally chaotic or when it consisted of a chaotic background with short-lived laminar domains. As chaotic domains became dominant, instantaneous fingering waves could be less correlated, so weak fluctuations could be expected in this case. We found, except for the early time decays, the general behavior of the G_{yy} is Gaussian.

We also performed similar experiments with $Ca = 0.491$. The same behaviour was observed in this case, but with smaller statistics.

3.5 Spatial autocorrelation function and length

Qualitatively, a spatial autocorrelation function describes the distance over which a property of a system persists. This is represented by a correlation length which is defined through the autocorrelation function, as given in Eq. (1.1) in Chapter 1. We now introduce the spatial autocorrelation function to probe the degree of disorder in a spatial pattern. From Eq. (1.1), we have

$$C'(\Delta x) = \frac{\langle \Delta I'(x,t)\Delta I'(x+\Delta x,t)\rangle}{\langle I'^2(x,t)\rangle} \tag{3.3}$$

where I' is the intensity at a spatial point in an instantaneous image (I' is different from I used in Eq. (3.1)) and $\Delta I' \equiv I'(x,t) - \langle I'(x,t)\rangle$. The $\langle\ \rangle$ denotes the ensemble average. $C'(\Delta x)$ tells us about the range of spatial correlations through the correlation length ξ. The computations are again performed on the central region of the patterns, $L/4 < x < 3L/4$, and averaged over 480 instantaneous images to get a smooth autocorrelation function. The autocorrelation function $C'(\Delta x)$ decays and oscillates with Δx. As illustrated in Fig 3.14, the oscillating tail can be well fitted by the product of a cosine and a decaying exponential, ignoring the point $C'(0) \equiv 1$. The behavior of the autocorrelation function agrees with that observed by Gluckman *et al.* [9] in the STC' region of the Faraday instability. Generally, the autocorrelation function can be fitted by

$$C'(\Delta x) = \eta \cos(k\Delta x) e^{-\frac{\Delta x}{\xi}} \tag{3.4}$$

where ξ is the spatial correlation length. Perfect correlation in the spatial domain means that the correlation length will be the same as the system length. Otherwise, the correlation length will be smaller. k is the mean wavenumber of the fingering pattern. η is a parameter giving the amplitude of $C'(\Delta x)$. The cosine function describes the periodic component of $C'(\Delta x)$. This periodic behavior is related to the period of the base fingering pattern. The correlation length ξ is the decay length of the exponential envelope and is determined from fits of the data to Eq. (3.4). The exponentially decaying envelope determined from the fit shown in Fig. 3.11 is plotted in the inset to Fig. 3.11, along with the amplitudes of the positive and negative peaks of $C'(\Delta x)$. The value of the decay length is 0.8 ± 0.1 cm which is approximately 1/5 of the dominant wavelength of the instantaneous fingering patterns, or 5% of the meniscus length. For low Ca_m we averaged the correlation lengths obtained from two successive 480 line images. The temporal auto correlation function of a single spatial point also shows exponential decay. Similar to the spatial decay length, the temporal decay length is fairly short in the STC regime. For Ca_m = 0.255 (the same parameter value as used in Fig. 3.11), ξ_t is about 0.17 ± 0.02 *s*.

In order to characterize the behavior we observed, we studied the variation of the decay length with capillary number Ca_m. Fig. 3.15 shows that ξ decreases as Ca_m increases. Each point in Fig. 3.15 was obtained from averaging over 960 individual calculations of the autocorrelation function. ξ decreases rapidly for Ca_m below 0.066. This corresponds to the first part of the STI region in which chaotic

domains develop in a laminar background, and shows that the development of the chaotic patches is very rapid as Ca_n is increased, *i.e.*, the degree of disorder increased dramatically. For large Ca_n, the rate of decrease of ξ slows. As shown in Fig. 3.16, the correlation length is fairly well described by a power law with a exponent of 0.37 ± 0.02 except in the vicinity of the threshold of the STC, where the behavior of ξ was unclear.

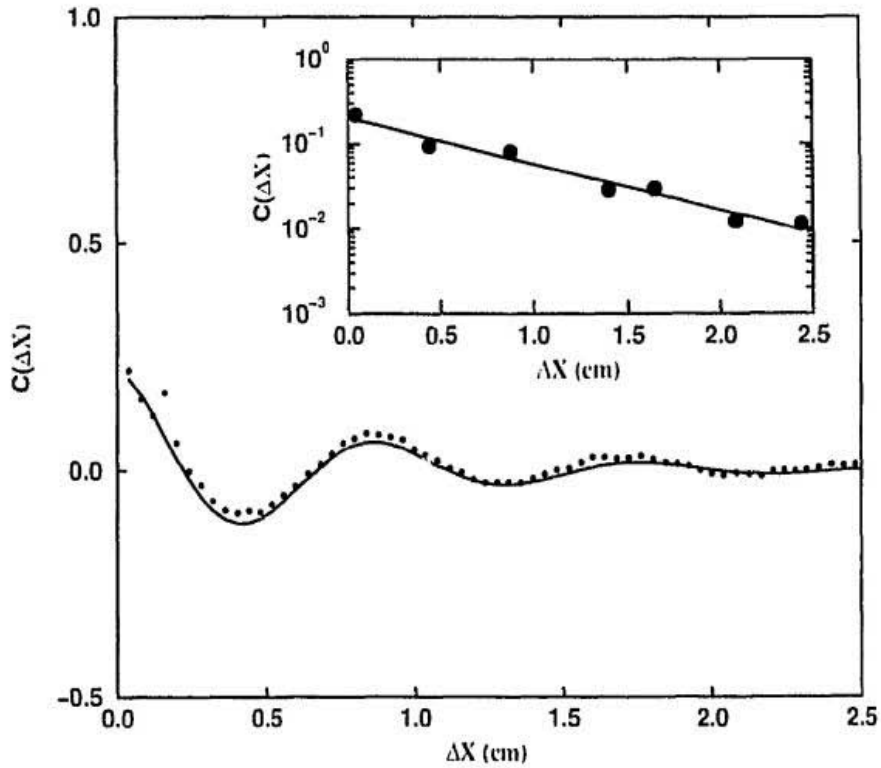

Figure 3.14: The spatial autocorrelation function for $Ca_1 = 0.689$ and $Ca_2 = 0.255$. The dots are the experimental data, and the solid line is a fitting line which is the product of a cosine and a decaying exponential. The inset is a semi log graph of the peaks of $C(\Delta x)$ along with the decaying exponential envelope determined from the fit shown in the main figure. The correlation length ξ is about 0.8 cm which is approximately 5% of the width of the front meniscus.

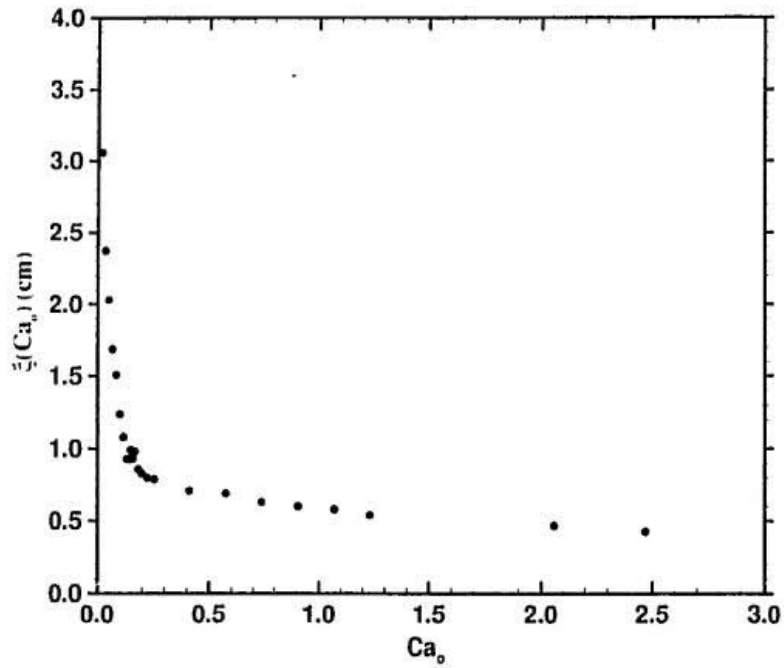

Figure 3.15: The spatial correlation length ξ decreases with an increase of the capillary number Ca_o.

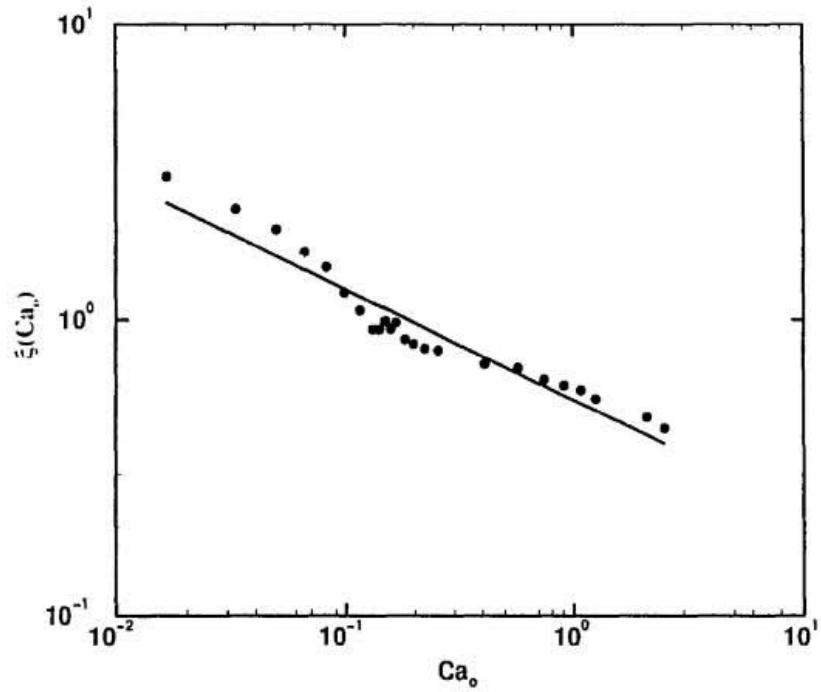

Figure 3.16: The log-log plot of the data shown in Fig. 3.16. The line is a power law with exponent $\mu = 0.37 \pm 0.02$.

Chapter 4

Discussion and Conclusion

4.1 Comparison with previous results

In this experiment, we have studied the statistics of 1D chaotic fingering patterns in several different ways. Some of our statistical results differ from those found from experiments on the Faraday instability by Gluckman *et al* [9]. These differences are mainly due to the different boundary conditions and experimental techniques involved.

Because the boundaries in the experiments of Gluckman *et al*. pin the phase of the pattern, their long time average shows a symmetric pattern. Based on the shadowgraph method they used for their system, they developed a simple one dimensional model, and then deduced a two dimensional model to interpret their 2D symmetric time averaged patterns. Ning *et al*. [28] also reported an ordered long time average in rotating thermal convection. They claimed that this symmetric averaged pattern is due to forcing from the boundary which produced a phase rigidity of the patterns. On the other hand, our experimental system has soft boundary conditions and this caused a structureless time averaged pattern.

To understand the symmetric structure in their long time average, Gluckman *et*

al. focused on probing the relationship between the long time average and instantaneous images, for example by calculating the spatial cross correlation coefficient between the time average and the instantaneous images. They found the time variation of this cross-correlation coefficient to be not far from Gaussian. In rotating thermal convection, Xing *et al.* did a similar investigation for the cross correlation of the instantaneous patterns and the averaged regular pattern. They found that the mean correlation C decreases as the system is driven further from equilibrium. They also studied the cross correlation between fluctuations of the patterns and the instantaneous heat transport of the system. Their cross correlations look qualitatively similar to each other. In our case, as the long time average and the instantaneous patterns are totally different, we studied the relationship among instantaneous images. We calculated the cross-correlation coefficient between instantaneous images, and found that the decay of C_{xx} at early times is generally exponential in both STI and STC regions. For $Ca_{\perp} > 0.40$, the early time decay of C_{xx} was too fast to be detected with the imaging system we used. The fluctuations of the temporal cross-correlation coefficient in our case are also Gaussian, except for the early time decays.

At $Ca_{\perp} = 0.1113$ (in the STC regime), the decay length is only about 80% of the wavelength of the base pattern, or 5% of the meniscus length. The decay length in Vihs-Kneen *et al.*'s paper [9] was much bigger than ours. At $\epsilon = 1$, their decay length is 2.0 ± 0.2 cm, which is about 6 times their dominant image wavelength or

20% of their container width. This difference may be the result of different dynamic systems involved. The short correlation length is expected, as in an infinite system there are usually many degrees of freedom involved. We observed that the spatial correlation length (decay length) decreases slowly in the STC regime. This is in agreement with Gluckman's observation in his experiment.

Furthermore, we calculated decay lengths at different Ca_n and found the decrease of the correlation length is approximately fitted by a power law, although the behavior is more complicated in the vicinity of the transition to STC. The slow decrease of the decay length in the STC region is understandable, as in the STC regime the characteristics of the disordered domains do not change dramatically with increasing Ca_n, so a slow decrease of correlation length is expected. Ning *et al.* did a similar investigation for the cross-correlation of the instantaneous patterns and the averaged regular pattern. They found that the mean correlation C decreases with increasing ϵ.

The rms difference between finite and infinite time averages of the chaotic patterns decays approximately as a power law. The results suggest that for short averaging times (i.e., less than about 50 s) the short time average approaches the long time average much like a Gaussian variable, but for longer averaging times the convergence is slower than that of a Gaussian. This is different from Gluckman's result, which shows a decay power law with an average exponent of 0.10 ± 0.03 [9].

4.2 Conclusion

In this work, we investigated the STC in printer's instability using various statistical measurements. Although none of our results are surprising, this work is a first step in the study of STC in the printer's instability.

The spatiotemporal chaos observed in the printer's instability with the speed of the inner cylinder fixed has been investigated. We have shown that fingering patterns driven out of equilibrium are spatiotemporally intermittent at low values of Ca_o and becomes fully chaotic as Ca_o is increased. We have shown that as a result of the soft boundary conditions on the ends of the pattern, the long time average of the spatially and temporally disordered 1D fingering patterns is structureless, in contrast to the results of Gluckman *et al.* for the Faraday instability. As our boundary conditions are perhaps closer to those which apply in some natural systems, our experimental results may be useful for understanding spatiotemporally chaotic dynamic patterns in nature. The convergence of the finite time average to infinite time average is slower than that of a Gaussian process for longer averaging times. This reveals that the time correlations decay more slowly than an exponential function.

The time-dependent cross-correlation coefficient C_{ij} between instantaneous images quantifies the time coherence between these images, and the behavior of $C_{ij}(t)$ shows how fast correlations are lost. The early time decays of C_{ij} show generally the exponential behavior in spite of the different dynamic states involved. On the whole, the decay constant increases with Ca_o. The fluctuations of C_{ij} beyond the

early time decay are Gaussian.

Both spatial and temporal autocorrelation functions have been calculated. The spatial autocorrelation function can be approximately fitted by the product of a cosine and a decaying exponential. The decay length is fairly short and decreases slowly in STC' regime. For Ca_c from 0.016 up to 2.47, the decrease of ξ can be fitted by a power law, though the behavior of ξ in the vicinity of the threshold of STC' is not clear. The behavior of the temporal autocorrelation function can be described by a decaying exponential. The correlation time is extremely short in STC' regime.

Future experimental work could be aimed at an investigation of the nucleation and elimination of defects in the STC' state, as this may eventually lead to an understanding of the origin of STC' in the printer's instability. Experiments with cylinders having ends which pin the phase of the fingering patterns might also be an interesting direction for the further study of the long time average of the STC' images.

Bibliography

[1] M.C. Cross and P.C. Hohenberg. *Reviews of Modern Physics*, **65 No. 3**, 1993.

[2] S. Ciliberto and P. Bigazzi. *Phys. Rev. Lett.*, **60**:286, 1988.

[3] M. Caponeri and S. Ciliberto. *Physica*, **58 D**:365, 1992.

[4] N.B. Tufillaro, R. Ramshankar, and J.P. Gollub. *Phys. Rev. Lett.*, **62**:422, 1989.

[5] M. Dubois, F. Daviaud, and M. Bonetitie. *Phys. Rev.*, **A 42**:3388, 1990.

[6] M. Dellnitz, M. Golubitsky, and I. Melbourne. In *Mechanisms of symmetry creation in Bifurcation and Symmetry*, page 99. (Birkhauser, Basel, 1992).

[7] P. Chossat and M. Golubitsky. *Physica*, **D(32)**:423, 1988.

[8] M. Dellnitz, M. Golubitsky, and I. Melbourne. *Archive for Rational Mechanics and Analysis*, **123**:75, 1993.

[9] B.J. Gluckman, C.B. Arnold, and J.P. Gollub. *Phys. Rev.*, **E 51**:1128, 1995.

[10] P. C. Hohenberg and B. I. Shraiman. *Physica*, **D 37**:109, 1989.

[11] S. W. Morris, E. Bodenschatz, D. S. Cannell, and G. Ahlers. *Phys. Rev. Lett.*, **13**:2026, 1993.

[12] P. Bergé. *Nucl. Phys.*, **B 2**:217, 1987.

[13] B. J. Gluckman, P. Marcq, J. Bridger, and J. P. Gollub. *Phys. Rev. Lett.*, **71(13)**:2034, 1993.

[14] C. D. Andereck, S. S. Liu, and H. Swinney. *J. Fluid Mech.*, **164**:155, 1986.

[15] I. Mutabazi, J. J. Hegseth, C. D. Andereck, and J. E. Wesfreid. *Phys. Rev. Lett.*, **64**:1729, 1990.

[16] I. Mutabazi and C. D. Andereck. *Phys. Rev. Lett.*, **70**:1129, 1993.

[17] M. Rabaud, S. Michalland, and Y. Couder. *Phys. Rev. Lett.*, **64**:184, 1990.

[18] H. Chaté and P. Manneville. *Phys. Rev. Lett.*, **58**:112, 1987.

[19] B. I. Shraiman, A. Pumir, W. Van Saarloos, P. C. Hohenberg, H. Chaté, and M. Holen. *Physica*, **D 57**:241, 1992.

[20] A. C. Newell, D. A. Rand, and D. Russell. *Physica*, **D 33**:281, 1988.

[21] G. Ahlers. In *Lectures in the Science of Complexity*, page 175. (Addison, Reading, 1989).

[22] M. Dubois and P. Bergé. *J. Fluid Mech.*, **85**:641, 1978.

[23] F. H. Busse. In *Hydrodynamic Instabilities and the Transition to Turbulence*, page 97. (Springer, Berlin, 1985).

[24] G. Ahlers, D. S. Cannell, and V. Steinberg. *Phys. Rev. Lett.*, **54**:1373, 1985.

[25] A. Pocheau, V. Croquette, and P. Le Gal. *Phys. Rev. Lett.*, **55**:1094, 1985.

[26] M. S. Heutmaker and J. P. Gollub. *Phys. Rev.*, **A 35**:242, 1987.

[27] F. Daviaud, M. Bonetti, and M. Dubois. *Physical Review*, **A 42**:3388, 1990.

[28] Li Xing, Y. Hu, R. E. Ecke, and G. Ahlers. *Phys. Rev. Lett.*, **71**:2246, 1993.

[29] M. Faraday. *Phil. Trans. R. Soc. Lond.*, **225**:298, 1831.

[30] T.B. Benjamin and F. Ursell. *Proc. Roy. Soc. London*, **A 225**:505, 1954.

[31] T.B. Benjamin and J.C. Scott. *J. Fluid Mech.*, **A 225**:241, 1979.

[32] J.G. Graham-Eagle. *Math. Proc. Camb. Phil. Soc.*, 94:553, 1983.

[33] R. Keolian, L.A. Turkevich, S.J. Putterman, I. Rudnick, and J.A. Rudnick. *Phys. Rev. Lett.*, **47**:1133, 1981.

[34] J.P. Gollub and C.W. Meyer. *Physica*, **D 6**:337, 1983.

[35] S. Ciliberto and J.P. Gollub. *Phys. Rev. Lett.*, **52**:922, 1984.

[36] S. Ciliberto and J.P. Gollub. *J. Fluid Mech.*, **158**:381, 1985.

[37] J. Wu, R. Keolian, and I. Rudnick. *Phys. Rev. Lett.*, **52**:1421, 1984.

[38] S. Douady and S. Fauve. *Europhys. Lett.*, **6**:221, 1988.

[39] S. Ciliberto, S. Douady, and S. Fauve. *Europhys. Lett.*, **15**:23, 1991.

[40] E. Pitts and G. Greiller. *J. Fluid Mech.*, **11**:33, 1961.

[11] G. I. Taylor. *J. Fluid Mech.*, **16**:595. 1963.

[12] J. R. A. Pearson. *J. Fluid Mech.*, **7**:181. 1960.

[13] C. C. Mill and G. R. South. *J. Fluid Mech.*, **28**:523. 1967.

[14] M. D. Savage. *J. Fluid Mech.*, **80**:743. 1977.

[15] M. D. Savage. *J. Fluid Mech.*, **80**:757. 1977.

[16] M. D. Savage. *J. Fluid Mech.*, **117**:143. 1982.

[17] H. Benkreira, M. F. Edwards, and W. L. Wilkinson. *Chem. Eng. Sci.*, **36**:429. 1981.

[18] K. J. Ruschak. *Ann. Rev. Fluid Mech.*, **17**:65. 1985.

[19] D. J. Coyle and C. W. Macosko. *J. Fluid Mech.*, **171**:183. 1986.

[50] D. J. Coyle, C. W. Macosko, and L. E. Scriven. *J. Fluid Mech.*, **216**:437. 1990.

[51] C. K. Aidun. *Tappi J.*, **74(3)**:213. 1991.

[52] S. Michalland. *Ph.D. Thesis, Université de Paris VI*. 1992 (unpublished).

[53] M. Raband and V. Hakim. In *Instabilities and Nonequilibrium Structures III*, page 217. (Kluwer Academic Publishers, 1991).

[54] M. Raband, Y. Couder, and S. Michalland. *Eur. J. Mech B/Fluids* **10**:253. 1991.

[55] L. Pan and J. R. de Bruyn. *Phys. Rev. Lett.*, **70**:12, 1992.

[56] L. Pan and J. R. de Bruyn. *Phys. Rev.*, **E** 49:1, 1994.

[57] L. Pan and J. R. de Bruyn. *Phys. Rev.*, **E** 49:3, 1994.

[58] L. Pan. Patterns and instabilities at a driven fluid air interface. *Ph. D. Thesis, Memorial University of Newfoundland*, 1993(unpublished).

[59] P. Coullet, R. E. Goldstein, and G. H. Gunaratne. *Phys. Rev. lett.*, **63**:1954, 1989.

[60] R. E. Goldstein, G. H. Gunaratne, L. Gil, and P. Coullet. *Phys. Rev.*, **A** **43**:6700, 1991.

[61] S. Fauve, S. Douady, and O. Thual. *J. Phys. (Paris)*, **II** (**1**):311, 1991.

[62] S. Michalland and M. Rabaud. *Physica*, **D** 61:197, 1992.

[63] S. Michalland, M. Rabaud, and Y. Couder. *Europhys. Lett.*, **22**(**1**):17, 1993.